

Measurement of the cosmic-ray flux from 2.5 EeV by the Pierre Auger Observatory after 19 years of operation

Diego Ravignani^{a,*} for the Pierre Auger Collaboration^c

^aITeDA (CNEA/CONICET/UNSAM), Argentina

^cObservatorio Pierre Auger, Av. San Martín Norte 304, 5613 Malargüe, Argentina

Full author list: https://www.auger.org/archive/authors_icrc_2025.html

E-mail: spokespersons@auger.org

We present the spectrum of cosmic rays with energies above 2.5 EeV measured at the Pierre Auger Observatory after 19 years of operation, covering the period before the AugerPrime upgrade. Two independent event sets from the surface array of 1500 m-spaced detectors are combined, yielding a total exposure of 104 900 km² sr yr. The first set includes events with zenith angles less than 60°, while the second consists of events between 60° and 80°, for which azimuthal asymmetries must be accounted for in the energy estimator. The threshold energy is chosen to ensure a trigger efficiency of the surface detector greater than 97%, thus minimizing composition biases. The energy scale is determined using high-quality fluorescence measurements, providing calorimetric estimates without reliance on simulations.

A statistically successful combination is achieved within the uncorrelated systematic uncertainties of the individual spectra. All spectra are consistent when analyzing potential declination dependences, except for a mild modulation expected from the previously reported dipolar anisotropy. In particular, this statement applies to the northernmost declination band [+24.8°, +44.8°], where only events with zenith angles between 60° and 80° contribute. Beyond the firmly established ankle and suppression spectral features, the combined spectrum across declinations -90° to +45° provides a measurement of the instep feature with more than 5 σ confidence.

*Speaker

1. Introduction

The Pierre Auger Observatory [1] has accumulated, since its beginning in 2004, the largest dataset of ultra-high-energy cosmic rays currently available. The volume and quality of the acquired data allowed us to measure a dipolar modulation of $\sim 6\%$ of an otherwise isotropic distribution of the arrival directions of cosmic rays with a significance greater than 5σ [2]. Motivated by the observed dipole, we previously searched for a modulation of the spectrum with declination [3, 4]. We recently conducted a more comprehensive search exploiting a $\sim 66\%$ larger exposure with a dataset that also includes events arriving with a zenith angle between 60° and 80° thus extending the declination reach from $+24.8^\circ$ to $+44.8^\circ$ [5] that is also reported here.

We present an energy spectrum using events observed by the water-Cherenkov detectors of the Surface Detector Array spaced at 1500 m during the 19 years of the Phase I data taken between January 1, 2004 and January 1, 2023. After this successful operation, the Observatory was upgraded, within a project named AugerPrime, with the goal of improving the measurement of the mass composition of ultra-high energy cosmic rays [6]. The upgrade includes new scintillator and radio detectors added in each position of the Surface Detector Array. We also upgraded the detector electronics to improve the timing and signal resolution of water-Cherenkov detectors and extended their dynamic range by adding a new PMT, smaller than the previous ones. We installed underground muon detectors at the positions of the 433 m and 750 m Surface Detector Arrays. Phase II data-taking started on April 1, 2023. We show a preliminary spectrum built with events acquired during the first two years of Phase II.

2. Vertical and inclined spectra

The depth of the water-Cherenkov detectors grants them the geometric acceptance needed to measure particles arriving at large zenith angles. However, the structure of the shower changes significantly for more vertical and inclined events. While the more vertical showers are symmetric around their axis and have a significant contribution at ground level of photons and electrons, the more inclined showers are composed predominantly of muons, and their axial symmetry is broken due to the geomagnetic field and other effects. Due to these reasons, we reconstruct the events arriving with a zenith angle up to 60° , denominated here as *vertical* events, with a different method than those arriving between 60° and 80° , the *inclined* events.

We reconstruct vertical events using a function that describes the fall-off of detector signals with the distance to the shower axis [7]. The value of this function at a distance of 1000 m ($S(1000)$) provides a measure of the shower size. We estimated a shower size independent of the zenith angle (S_{38}), equivalent to the size the shower would have had if it had arrived at a zenith angle of 38° , via an attenuation function, $S_{38} = S(1000) / f_{\text{att}}$, calculated with the Constant Intensity Cut method [8]. The attenuation function f_{att} depends on the zenith angle through a variable $x = \sin^2 \theta - \sin^2 38^\circ$ and on S_{38} through a variable $y = \log_{10}(S_{38}/S_0)$, with $S_0 = 40$ VEM, and

$$f_{\text{att}}(x, y) = 1 + \sum_{i=1}^3 \sum_{j=0}^2 a_{ij} x^i y^j, \quad (1)$$

with parameters a_{ij} in the Table 1.

Table 1: Coefficients of the attenuation function used to correct the shower size of vertical events.

	1	y	y^2
x	-0.936	-0.005	0.4
x^2	-1.62	-0.51	-0.13
x^3	0.92	-0.54	-1.75

The shower size S_{38} is calibrated with the energy measured with the telescopes of the Fluorescence Detector (E_{FD}) using high-quality events observed in coincidence with the Surface Detector Array. From calibration data, we establish the relationship between the cosmic ray energy and the shower size, $E = AS_{38}^B$, with $A = (186 \pm 3)$ PeV, $B = 1.021 \pm 0.004$, and a correlation coefficient between A and B , $\rho = -0.98$.

We reconstruct inclined events by fitting a function that describes the signal pattern [9, 10]. This map is scaled with the ratio of the measured and simulated shower size at 10 EeV (N_{19}). The parameter N_{19} attenuates with the zenith angle in a slightly model-dependent way, in particular, due to the residual contribution of photons and electrons. This attenuation is corrected using the Constant Intensity Cut method as in the case of vertical events to derive an equivalent shower size at 68° , $N_{68} = N_{19}/f_{\text{att}}$. The attenuation function is described as a simplified model of Eq. 1, with $x = \sin^2 \theta - \sin^2 68^\circ$, $y = \log_{10}(N_{19})$, and $f_{\text{att}} = 1 + (0.292 - 0.468 y) x + (-4.96 + 0.79 y) x^2$. The shower size N_{68} is calibrated in energy using events observed in coincidence with the Fluorescence Detector as with vertical events. The energy of inclined events is calculated from $E = A N_{68}^B$, with $A = (5.29 \pm 0.06)$ EeV, $B = 1.046 \pm 0.014$, and a correlation coefficient $\rho_{AB} = -0.66$.

We calibrated the events using a Fluorescence Detector reconstruction updated with an improved estimation of aerosol attenuation and parametrization of the longitudinal profile of light emission [11]. We calibrated the vertical and inclined events with the same fluorescence reconstruction so that both datasets share the same energy scale. The systematic uncertainty of the energy of vertical and inclined events is driven by the absolute energy scale of fluorescence detection (14%) [12] that is correlated between both data sets. In addition, the uncertainty of the calibration parameters propagates as another source of systematic uncertainty in the energy but is not correlated between vertical and inclined events. Although the number of events available in the vertical calibration renders this source of systematic uncertainty negligible, inclined energies with fewer calibration events have a systematic uncertainty of about 2%.

For the spectrum based on vertical events, we selected events that have the detector with the highest signal surrounded by six working detectors to ensure the energy is well reconstructed. We applied a similar condition for inclined events, requiring the reconstructed core to be contained within a hexagon of six working detectors. We choose the energy thresholds of the vertical spectrum at $\log_{10}(E/\text{eV}) = 18.4$ ($E \sim 2.5$ EeV), and of the inclined spectrum at $\log_{10}(E/\text{eV}) = 18.6$ ($E \sim 4$ EeV), limits at which the trigger efficiency exceeds 97% [13]. Above the energy threshold, the exposure is constant and is calculated by monitoring the status of the detectors every 1 s. From this thorough monitoring, we identified periods of unstable acquisition that accounted for less than 3% of the observation time. We excluded the events observed during these periods and penalized the exposure accordingly. We computed an exposure of $(81\,100 \pm 700)$ km² sr yr for the vertical spectrum and $(23\,800 \pm 400)$ km² sr yr for the inclined spectrum.

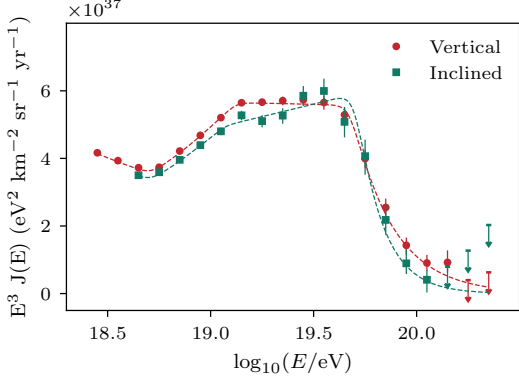


Figure 1: Vertical spectrum using events arriving with a zenith angle less than 60° , and inclined spectrum from events with a zenith angle between 60° and 80° . The spectrum data corrected for the detector response and the fitted flux are shown. No cut in the declination of the arrival direction has been applied.

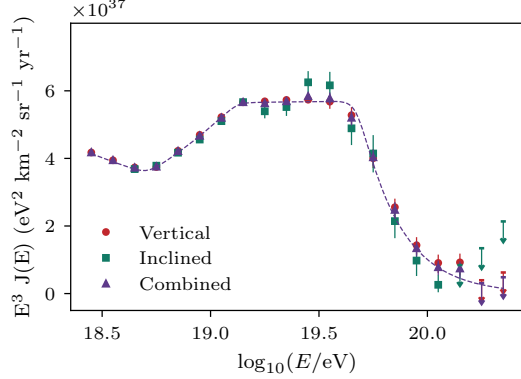


Figure 2: Vertical and inclined spectra in their common declination band $[-84.8^\circ, +24.8^\circ]$. The inclined spectrum is shifted according to the recalibrated event energies calculated in the spectra combination. The resulting combined spectrum is shown.

We fitted the spectrum data with a flux of cosmic rays modeled as a power-law function with smooth transitions,

$$J(E) = J_0 \left(\frac{E}{E_0} \right)^{-\gamma_0} \frac{\prod_{i=1}^3 \left[1 + \left(\frac{E}{E_i} \right)^{\omega_i^{-1}} \right]^{(\gamma_i - \gamma_{i+1}) \omega_i}}{\prod_{i=1}^3 \left[1 + \left(\frac{E_0}{E_i} \right)^{\omega_i^{-1}} \right]^{(\gamma_i - \gamma_{i+1}) \omega_i}}, \quad (2)$$

with the reference energy E_0 set at $10^{0.5} \sim 3.16$ EeV and the three transitions widths fixed at $\omega_i = 0.05$. We fitted the flux normalization J_0 , the ankle energy E_1 , the instep energy E_2 , the fall-off energy E_3 , and the four spectral indexes γ_i . The spectral index γ_1 corresponds to the region before the ankle, γ_2 between the ankle and the instep, and likewise for the other spectral indexes.

The observed number of events in each energy bin is affected, besides the prediction arising from the cosmic ray flux, by the effect of the detector response that includes the trigger efficiency, and the bias and finite resolution of the reconstructed energy [3]. We incorporated these effects in the spectrum fitting. We correspondingly corrected the observed flux in each bin by factors $c_i \sim [0.9 - 1]$, $J'_i = c_i J_i$, with $J_i = N_i / (\varepsilon \Delta E_i)$, with N_i the observed number of events, and ΔE_i the energy difference between the bin limits. The vertical and inclined spectra corrected by the detector response and the corresponding fitted fluxes are shown in Fig. 1.

3. Dependency of the flux with declination

The latitude of the Observatory at 35.2° S permits the observation of cosmic rays arriving with a declination from the south celestial pole up to $+24.8^\circ$ with vertical events, and the range $[-84.8^\circ, +44.8^\circ]$ with inclined events. We exploited the cumulative exposure of the vertical and

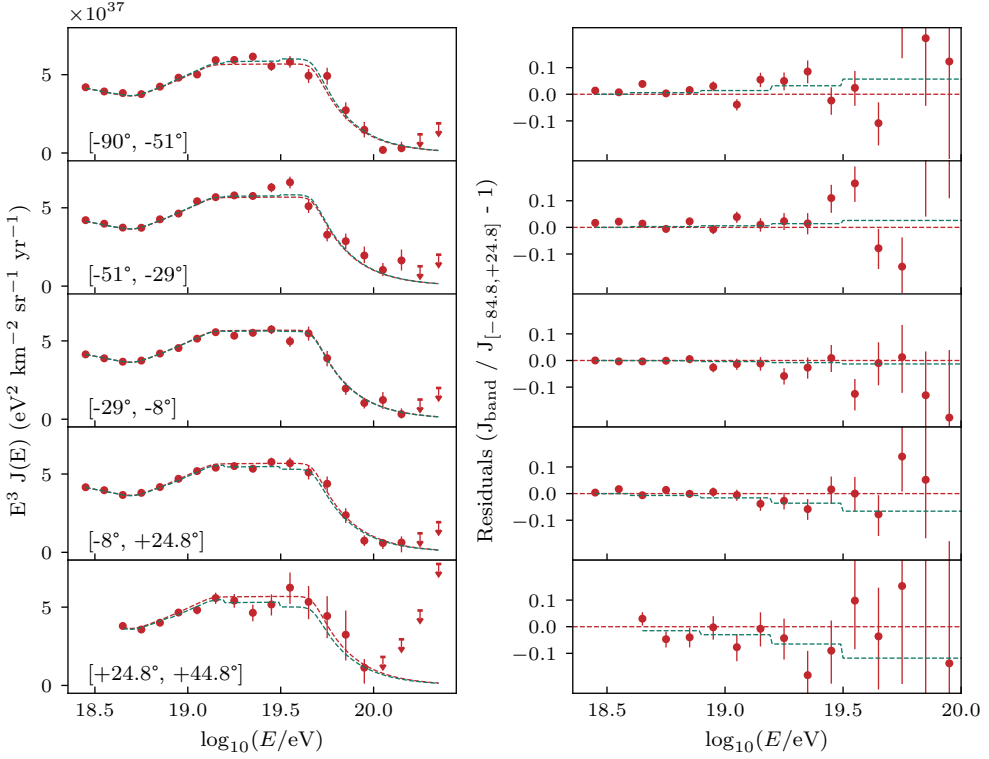


Figure 3: Left panel: Spectra in five declination bands combining vertical and inclined events. The flux fitted in the common declination band $[-84.8^\circ, +24.8^\circ]$ is shown in red, and the flux modulated by the dipole of the arrival direction distribution is shown in green. Right panel: Residuals of the combined spectra and the fitted flux in each declination band clipped to $[-0.25, 0.25]$.

inclined spectra by combining them into a single spectrum. To guarantee the observation of the same sky, we combined them in their common field of view given by the declination band $[-84.8^\circ, +24.8^\circ]$ using the method in reference [14]. We fitted the vertical and inclined data simultaneously with the flux model (2).

During the fit, we included the effect of the uncorrelated systematics on the energy of the vertical and inclined events. We fixed the energies resulting from the calibration for the vertical events as they have negligible systematics. However, we fluctuated the energy of inclined events by varying the parameters A and B around the calibration estimates. We use different B deviations for energies below and above 10 EeV, and denominated them δB and δC , respectively, to account for possible deviations of the inclined calibration from a pure power-law model originated, for example, by the evolution of the primary composition. The combination maximizes a Poisson likelihood that contains contributions predicting the expected number of events in each bin of the vertical and inclined spectra. In addition, during the fit, we penalized the deviations from the calibration estimates (δA , δB , and δC).

We fitted simultaneously the eight spectral parameters and the three calibration parameters. The fitted deviations are $\delta A = (160 \pm 39) \text{ PeV}$, $\delta B = 0.003 \pm 0.016$, and $\delta C = -0.02 \pm 0.02$. The recalibration of inclined events increases the energy by 2.9% at 4 EeV, 3.1% at 10 EeV, and decreases it 1% at 100 EeV. For the combination we obtained a deviance $D = 40.5$, for which we

Table 2: Spectral parameters of Phase I spectrum including the energy of the ankle (E_1), the instep (E_2), and the flux suppression (E_3), and the spectral indexes γ .

Parameter	Value	σ_{stat}	σ_{sys}	Parameter	Value	σ_{stat}	σ_{sys}
J_0 ($\text{km}^{-2}\text{sr}^{-1}\text{yr}^{-1}\text{eV}^{-1}$)	1.269	0.003	0.40	γ_1	3.26	0.01	0.10
E_1 (EeV)	5.1	0.1	1.1	γ_2	2.51	0.03	0.05
E_2 (EeV)	13	1	2	γ_3	2.99	0.03	0.10
E_3 (EeV)	48	2	5	γ_4	5.4	0.2	0.1

estimated a p -value $\simeq 0.12$. We show in Fig. 2 the fitted flux and the combined spectrum calculated in each bin as,

$$J_i = \frac{c_i n_i + c'_i n'_i}{(\varepsilon + \varepsilon') \Delta E_i}, \quad (3)$$

with the unprimed and primed symbols corresponding to the vertical and inclined spectra.

We searched for a dependence of the spectrum with declination by dividing the sky into five declination bands. We divided the range observed with vertical events $[-90^\circ, +24.8^\circ]$ in four bands of similar exposure. In addition, we considered a northern band $[+24.8^\circ, +44.8^\circ]$ observed only with inclined events. We compared the spectra in each declination band with the flux in the common declination range $[-84.8^\circ, +24.8^\circ]$. We calculated the combined spectrum in each band as per Eq. 3 using the number of events and exposures of each band. We show the spectra in declination bands and the flux in the left panel of Fig. 3. We also show the flux expected in each band when the modulations given by the dipole in the arrival directions observed by Auger are considered. We show in the right panel of Fig. 3 the residuals of the spectra in declination bands with respect to the fitted flux and the deviations of the flux modulated by the dipole. The residuals follow the trend imprinted by the dipole between 4 EeV and 32 EeV, and statistical uncertainties dominate beyond 32 EeV. The agreement of the dipole modulation with the spectra in each band is expected since the anisotropy and spectrum data sets overlap considerably.

4. Phase I spectrum

Given that the spectra in the different declination bands agree with the flux fitted in the common declination band within statistical uncertainties, we combine the vertical and inclined into a single spectrum. While in section 3 we restricted the vertical and inclined spectra to their common declination band $[-84.8^\circ, +24.8^\circ]$, we now combine them at all observed declinations, reaching a total exposure of $104\,900 \text{ km}^2 \text{ sr yr}$ corresponding to the sum of the exposure of the vertical and inclined datasets. The combined spectrum is calculated using Eq. 3 after shifting the inclined spectrum with the parameters calculated in section 3. We show the combined spectrum and the corresponding fit in Fig. 4, and the spectrum data are provided in [5]. The shaded band represents the systematic uncertainty of the flux, which is dominated by the systematic uncertainty of the energy scale. The flux exhibits the firmly established features of the ankle and suppression, as well as the instep, which we unveiled with a significance of 3.9σ in 2020 [3]. Table 2 contains the fitted spectral parameters and their statistical and systematic uncertainties.

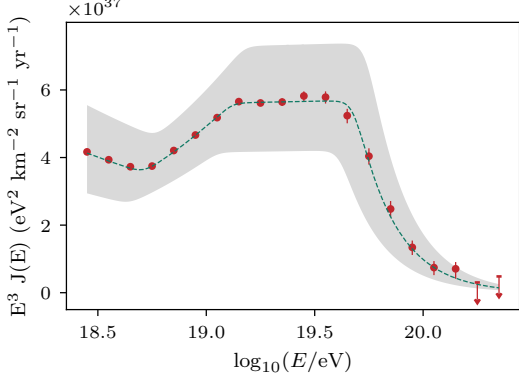


Figure 4: Combined spectrum using events arriving with zenith angle up to 80° observed at declinations from the south celestial pole up to $+44.8^\circ$. The systematic flux uncertainty is shown as a shaded band.

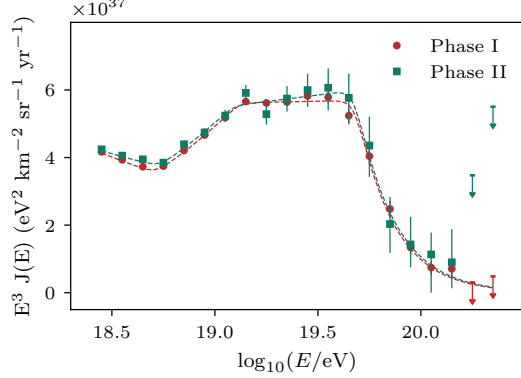


Figure 5: Preliminary spectrum using events arriving with zenith angle up to 60° observed during the second phase of Auger. The spectrum of Phase I is shown for comparison.

To assess the significance of the instep with the larger dataset currently available, we sampled energies from a reference model, which contained a slow suppression instead of the instep. We fitted the sampled data with the reference model and alternative one containing the instep and built a test statistic as the ratio of their respective likelihoods. The estimated significance is based on the number of times the sampled test statistic is greater than the one calculated by fitting the observed data. The test statistic was larger than the observed value ($t_{\text{obs}} \sim 35$) in only two out of 10^8 simulations, corresponding to a significance of 5.5σ .

5. Preliminary Phase II spectrum

In this section, we present a preliminary spectrum built from vertical events observed during the second Phase of the Auger Observatory, using data recorded from April 1, 2023, to March 1, 2025. To provide this first view of the Phase II spectrum, we reconstructed the events using the Phase I setup. For example, we applied the same lateral distribution function, attenuation with zenith angle, energy calibration, and detector response model used to unfold the spectrum. We also use the same method as in Phase I to select spectrum events, excluding periods of unstable data-taking, and to calculate the exposure. The exposure during the data-taking considered was $(9200 \pm 300) \text{ km}^2 \text{ sr yr}$, about 10% of the Phase I spectrum. Reusing the Phase I analysis was possible because the upgrade of the Observatory was designed so that water-Cherenkov detectors were backwards compatible.

We show in Fig. 5 the spectra of Phase I and II. We evaluated the consistency of Phase I and Phase II spectra with a Fisher's test that combines chi-square tests for bins with many events with exact binomial tests for bins with few events [15]. We assumed a systematic uncertainty of 1% uncorrelated between the two spectra, a conservative estimate given the 3% exposure uncertainty.

The observed Fisher's test statistic was $t = 38.0$ for 36 degrees of freedom, corresponding to a p-value $p = 0.30$ estimated numerically with Monte Carlo simulations.

We fitted the Phase II spectrum with the Phase I model, and obtained spectral parameters that are in agreement with the values in Table 2 within the statistical uncertainties. We will customize the event reconstruction to accommodate the improvements of the water-Cherenkov detectors in Phase II, but this early analysis already shows that minor changes to the existing setup will be required. In the future, we will use Phase I and II events to build a single spectrum with the combined exposure achieved during the complete lifetime of the Pierre Auger Observatory.

6. Conclusions

We presented an updated spectrum measured with the 1500 m Surface Detector Array of the Pierre Auger Observatory using events arriving with zenith angles up to 80° . The data set comprises 19 years of Phase I data taken from 2004 to 2023 with an exposure of $(104\,900 \pm 3000) \text{ km}^2 \text{ sr yr}$, enabling the discovery-level observation of the spectrum instep at $(13 \pm 1 \pm 2) \text{ EeV}$ with the spectral index increasing from $2.51 \pm 0.03^{\text{stat}} \pm 0.05^{\text{sys}}$ to $2.99 \pm 0.03^{\text{stat}} \pm 0.10^{\text{sys}}$. We did not find any statistically significant dependence of the flux with declination from the south celestial pole up to a $+44.8^\circ$, bar a small trend consistent with the well-established dipolar anisotropy in arrival directions. Finally, we presented for the first time a spectrum obtained with events measured during Phase II of the Auger Observatory, showing its consistency with the Phase I spectrum.

References

- [1] A. Aab *et al.* (Pierre Auger), *Nucl. Instrum. Meth. A* **798**, 172 (2015), arXiv:1502.01323 [astro-ph.IM]
- [2] A. A. Halim *et al.* (Pierre Auger), *Astrophys. J.* **976**, 48 (2024), arXiv:2408.05292 [astro-ph.HE].
- [3] A. Aab *et al.* (Pierre Auger), *Phys. Rev. D* **102**, 062005 (2020), arXiv:2008.06486 [astro-ph.HE].
- [4] A. Aab *et al.* (Pierre Auger), *Phys. Rev. Lett.* **125**, 121106 (2020), arXiv:2008.06488 [astro-ph.HE].
- [5] A. Abdul Halim *et al.* (Pierre Auger), PoS (2025), arXiv:2506.11688 [astro-ph.HE].
- [6] D. Schmidt (Pierre Auger), in *these proceedings*.
- [7] A. Aab *et al.* (Pierre Auger), *JINST* **15** (10), P10021, arXiv:2007.09035 [astro-ph.IM].
- [8] J. Hersil, I. Escobar, D. Scott, G. Clark, and S. Olbert, *Phys. Rev. Lett.* **6**, 22 (1961).
- [9] A. Aab *et al.* (Pierre Auger), *JCAP* **2014** (08), 019, arXiv:1407.3214 [astro-ph.HE].
- [10] A. Aab *et al.* (Pierre Auger), *JCAP* **2015** (08), 049, arXiv:1503.07786 [astro-ph.HE].
- [11] B. R. Dawson *et al.* (Pierre Auger), *EPJ Web Conf.* **197**, 01004 (2019).
- [12] V. Verzi (Pierre Auger), in *33rd International Cosmic Ray Conference* (2013) p. 0928.
- [13] J. Abraham *et al.* (Pierre Auger), *Nucl. Instrum. Meth. A* **613**, 29 (2010), arXiv:1111.6764 [astro-ph.IM].
- [14] P. Abreu *et al.* (Pierre Auger), *Eur. Phys. J. C* **81**, 966 (2021), arXiv:2109.13400 [astro-ph.HE].
- [15] D. Ravignani (Pierre Auger), *PoS UHECR2024*, 038 (2025).

The Pierre Auger Collaboration



PIERRE
AUGER
OBSERVATORY

- A. Abdul Halim¹³, P. Abreu⁷⁰, M. Aglietta^{53,51}, I. Allekotte¹, K. Almeida Cheminant^{78,77}, A. Almela^{7,12}, R. Aloisio^{44,45}, J. Alvarez-Muñiz⁷⁶, A. Ambrosone⁴⁴, J. Ammerman Yebra⁷⁶, G.A. Anastasi^{57,46}, L. Anchordoqui⁸³, B. Andrade⁷, L. Andrade Dourado^{44,45}, S. Andringa⁷⁰, L. Apollonio^{58,48}, C. Aramo⁴⁹, E. Arnone^{62,51}, J.C. Arteaga Velázquez⁶⁶, P. Assis⁷⁰, G. Avila¹¹, E. Avocone^{56,45}, A. Bakalova³¹, F. Barbato^{44,45}, A. Bartz Mocellin⁸², J.A. Bellido¹³, C. Berat³⁵, M.E. Bertaina^{62,51}, M. Bianciotto^{62,51}, P.L. Biermann^a, V. Binet⁵, K. Bismarck^{38,7}, T. Bister^{77,78}, J. Biteau^{36,i}, J. Blazek³¹, J. Blümner⁴⁰, M. Boháčová³¹, D. Boncioli^{56,45}, C. Bonifazi⁸, L. Bonneau Arbeletche²², N. Borodai⁶⁸, J. Brack^f, P.G. Brichetto Orcher^{7,40}, F.L. Briechle⁴¹, A. Bueno⁷⁵, S. Buitink¹⁵, M. Buscemi^{46,57}, M. Büskens^{38,7}, A. Bwembya^{77,78}, K.S. Caballero-Mora⁶⁵, S. Cabana-Freire⁷⁶, L. Caccianiga^{58,48}, F. Campuzano⁶, J. Caraça-Valente⁸², R. Caruso^{57,46}, A. Castellina^{53,51}, F. Catalani¹⁹, G. Cataldi⁴⁷, L. Cazon⁷⁶, M. Cerda¹⁰, B. Čermáková⁴⁰, A. Cermenati^{44,45}, J.A. Chinellato²², J. Chudoba³¹, L. Chytha³², R.W. Clay¹³, A.C. Cobos Cerutti⁶, R. Colalillo^{59,49}, R. Conceição⁷⁰, G. Consolati^{48,54}, M. Conte^{55,47}, F. Convenga^{44,45}, D. Correia dos Santos²⁷, P.J. Costa⁷⁰, C.E. Covault⁸¹, M. Cristinziani⁴³, C.S. Cruz Sanchez³, S. Dasso^{4,2}, K. Daumiller⁴⁰, B.R. Dawson¹³, R.M. de Almeida²⁷, E.-T. de Boone⁴³, B. de Errico²⁷, J. de Jesús⁷, S.J. de Jong^{77,78}, J.R.T. de Mello Neto²⁷, I. De Mitri^{44,45}, J. de Oliveira¹⁸, D. de Oliveira Franco⁴², F. de Palma^{55,47}, V. de Souza²⁰, E. De Vito^{55,47}, A. Del Popolo^{57,46}, O. Deligny³³, N. Denner³¹, L. Deval^{53,51}, A. di Matteo⁵¹, C. Dobrigkeit²², J.C. D'Olivo⁶⁷, L.M. Domingues Mendes^{16,70}, Q. Dorost⁴³, J.C. dos Anjos¹⁶, R.C. dos Anjos²⁶, J. Ebr³¹, F. Ellwanger⁴⁰, R. Engel^{38,40}, I. Epicoco^{55,47}, M. Erdmann⁴¹, A. Etchegoyen^{7,12}, C. Evoli^{44,45}, H. Falcke^{77,79,78}, G. Farrar⁸⁵, A.C. Fauth²², T. Fehler⁴³, F. Feldbusch³⁹, A. Fernandes⁷⁰, M. Fernandez¹⁴, B. Fick⁸⁴, J.M. Figueira⁷, P. Filip^{38,7}, A. Filipčič^{74,73}, T. Fitoussi⁴⁰, B. Flagg⁸⁷, T. Fodran⁷⁷, A. Franco⁴⁷, M. Freitas⁷⁰, T. Fujii^{86,h}, A. Fuster^{7,12}, C. Galea⁷⁷, B. García⁶, C. Gaudí³⁷, P.L. Ghia³³, U. Giaccari⁴⁷, F. Gobbi¹⁰, F. Gollan⁷, G. Golup¹, M. Gómez Berisso¹, P.F. Gómez Vitale¹¹, J.P. Gongora¹¹, J.M. González¹, N. González⁷, D. Góra⁶⁸, A. Gorgi^{53,51}, M. Gottowik⁴⁰, F. Guarino^{59,49}, G.P. Guedes²³, L. Gülow⁴⁰, S. Hahn³⁸, P. Hamal³¹, M.R. Hampel⁷, P. Hansen³, V.M. Harvey¹³, A. Haungs⁴⁰, T. Hebbeker⁴¹, C. Hojvat^d, J.R. Hörandel^{77,78}, P. Horvath³², M. Hrabovsky³², T. Huege^{40,15}, A. Insolia^{57,46}, P.G. Isar⁷², M. Ismaiel^{77,78}, P. Janecek³¹, V. Jilek³¹, K.-H. Kampert³⁷, B. Keilhauer⁴⁰, A. Khakurdi⁷⁷, V.V. Kizakke Covilakam^{7,40}, H.O. Klages⁴⁰, M. Kleifges³⁹, J. Köhler⁴⁰, F. Krieger⁴¹, M. Kubatova³¹, N. Kunka³⁹, B.L. Lago¹⁷, N. Langner⁴¹, N. Leal⁷, M.A. Leigui de Oliveira²⁵, Y. Lema-Capeans⁷⁶, A. Letessier-Selvon³⁴, I. Lhenry-Yvon³³, L. Lopes⁷⁰, J.P. Lundquist⁷³, M. Mallamaci^{60,46}, D. Mandat³¹, P. Mantsch^d, F.M. Mariani^{58,48}, A.G. Mariazzi³, I.C. Marić¹⁴, G. Marsella^{60,46}, D. Martello^{55,47}, S. Martinelli^{40,7}, M.A. Martins⁷⁶, H.-J. Mathes⁴⁰, J. Matthews^g, G. Matthiae^{61,50}, E. Mayotte⁸², S. Mayotte⁸², P.O. Mazur^d, G. Medina-Tanco⁶⁷, J. Meinert³⁷, D. Melo⁷, A. Menshikov³⁹, C. Merx⁴⁰, S. Michal³¹, M.I. Micheletti⁵, L. Miramonti^{58,48}, M. Mogarkar⁶⁸, S. Mollerach¹, F. Montanet³⁵, L. Morejon³⁷, K. Mulrey^{77,78}, R. Mussa⁵¹, W.M. Namasaka³⁷, S. Negi³¹, L. Nellen⁶⁷, K. Nguyen⁸⁴, G. Nicora⁹, M. Niechciol⁴³, D. Nitz⁸⁴, D. Nosek³⁰, A. Novikov⁸⁷, V. Novotny³⁰, L. Nožka³², A. Nucita^{55,47}, L.A. Núñez²⁹, J. Ochoa^{7,40}, C. Oliveira²⁰, L. Östman³¹, M. Palatka³¹, J. Pallotta⁹, S. Panja³¹, G. Parente⁷⁶, T. Paulsen³⁷, J. Pawlowsky³⁷, M. Pech³¹, J. Pěkala⁶⁸, R. Pelayo⁶⁴, V. Pelgrims¹⁴, L.A.S. Pereira²⁴, E.E. Pereira Martins^{38,7}, C. Pérez Bertolli^{7,40}, L. Perrone^{55,47}, S. Petrera^{44,45}, C. Petrucci⁵⁶, T. Pierog⁴⁰, M. Pimenta⁷⁰, M. Platino⁷, B. Pont⁷⁷, M. Pourmohammad Shahvar^{60,46}, P. Privitera⁸⁶, C. Priyadarshi⁶⁸, M. Prouza³¹, K. Pytel⁶⁹, S. Querchfeld³⁷, J. Rautenberg³⁷, D. Ravignani⁷, J.V. Reginatto Akim²², A. Reuzki⁴¹, J. Ridky³¹, F. Riehn^{76,j}, M. Risse⁴³, V. Rizi^{56,45}, E. Rodriguez^{7,40}, G. Rodriguez Fernandez⁵⁰, J. Rodriguez Rojo¹¹, S. Rossoni⁴², M. Roth⁴⁰, E. Roulet¹, A.C. Rovero⁴, A. Saftoiu⁷¹, M. Saharan⁷⁷, F. Salamida^{56,45}, H. Salazar⁶³, G. Salina⁵⁰, P. Sampathkumar⁴⁰, N. San Martin⁸², J.D. Sanabria Gomez²⁹, F. Sánchez⁷, E.M. Santos²¹, E. Santos³¹, F. Sarazin⁸², R. Sarmento⁷⁰, R. Sato¹¹, P. Savina^{44,45}, V. Scherini^{55,47}, H. Schieler⁴⁰, M. Schimassek³³, M. Schimp³⁷, D. Schmidt⁴⁰, O. Scholten^{15,b}, H. Schoorlemmer^{77,78}, P. Schovánek³¹, F.G. Schröder^{87,40}, J. Schulte⁴¹, T. Schulz³¹, S.J. Sciutto³, M. Scornavacche⁷, A. Sedoski⁷, A. Segreto^{52,46}, S. Sehgal³⁷, S.U. Shivashankara⁷³, G. Sigl⁴², K. Simkova^{15,14}, F. Simon³⁹, R. Šmídá⁸⁶, P. Sommers^e, R. Squartini¹⁰, M. Stadelmaier^{40,48,58}, S. Stanić⁷³, J. Stasielak⁶⁸, P. Stassi³⁵, S. Strähn³⁸, M. Straub⁴¹, T. Suomijärvi³⁶, A.D. Supanitsky⁷, Z. Svozilikova³¹, K. Syrokvas³⁰, Z. Szadkowski⁶⁹, F. Tairli¹³, M. Tambone^{59,49}, A. Tapia²⁸, C. Taricco^{62,51}, C. Timmermans^{78,77}, O. Tkachenko³¹, P. Tobiska³¹, C.J. Todero Peixoto¹⁹, B. Tomé⁷⁰, A. Travaíni¹⁰, P. Travnicek³¹, M. Tueros³, M. Unger⁴⁰, R. Uzeiroska³⁷, L. Vaclavek³², M. Vacula³², I. Vaiman^{44,45}, J.F. Valdés Galicia⁶⁷, L. Valore^{59,49}, P. van Dillen^{77,78}, E. Varela⁶³, V. Vašíčková³⁷, A. Vásquez-Ramírez²⁹, D. Veberič⁴⁰, I.D. Vergara Quispe³, S. Verpoest⁸⁷, V. Verzi⁵⁰, J. Vicha³¹, J. Vink⁸⁰, S. Vorobiov⁷³, J.B. Vuta³¹, C. Watanabe²⁷, A.A. Watson^c, A. Weindl⁴⁰, M. Weitz³⁷, L. Wiencke⁸², H. Wilczyński⁶⁸, B. Wundheiler⁷, B. Yue³⁷, A. Yushkov³¹, E. Zas⁷⁶, D. Zavrtanik^{73,74}, M. Zavrtanik^{74,73}

- ¹ Centro Atómico Bariloche and Instituto Balseiro (CNEA-UNCuyo-CONICET), San Carlos de Bariloche, Argentina
² Departamento de Física and Departamento de Ciencias de la Atmósfera y los Océanos, FCEyN, Universidad de Buenos Aires and CONICET, Buenos Aires, Argentina
³ IFLP, Universidad Nacional de La Plata and CONICET, La Plata, Argentina
⁴ Instituto de Astronomía y Física del Espacio (IAFE, CONICET-UBA), Buenos Aires, Argentina
⁵ Instituto de Física de Rosario (IFIR) – CONICET/U.N.R. and Facultad de Ciencias Bioquímicas y Farmacéuticas U.N.R., Rosario, Argentina
⁶ Instituto de Tecnologías en Detección y Astropartículas (CNEA, CONICET, UNSAM), and Universidad Tecnológica Nacional – Facultad Regional Mendoza (CONICET/CNEA), Mendoza, Argentina
⁷ Instituto de Tecnologías en Detección y Astropartículas (CNEA, CONICET, UNSAM), Buenos Aires, Argentina
⁸ International Center of Advanced Studies and Instituto de Ciencias Físicas, ECyT-UNSAM and CONICET, Campus Miguelete – San Martín, Buenos Aires, Argentina
⁹ Laboratorio Atmósfera – Departamento de Investigaciones en Láseres y sus Aplicaciones – UNIDEF (CITEDEF-CONICET), Argentina
¹⁰ Observatorio Pierre Auger, Malargüe, Argentina
¹¹ Observatorio Pierre Auger and Comisión Nacional de Energía Atómica, Malargüe, Argentina
¹² Universidad Tecnológica Nacional – Facultad Regional Buenos Aires, Buenos Aires, Argentina
¹³ University of Adelaide, Adelaide, S.A., Australia
¹⁴ Université Libre de Bruxelles (ULB), Brussels, Belgium
¹⁵ Vrije Universiteit Brussels, Brussels, Belgium
¹⁶ Centro Brasileiro de Pesquisas Fisicas, Rio de Janeiro, RJ, Brazil
¹⁷ Centro Federal de Educação Tecnológica Celso Suckow da Fonseca, Petropolis, Brazil
¹⁸ Instituto Federal de Educação, Ciência e Tecnologia do Rio de Janeiro (IFRJ), Brazil
¹⁹ Universidade de São Paulo, Escola de Engenharia de Lorena, Lorena, SP, Brazil
²⁰ Universidade de São Paulo, Instituto de Física de São Carlos, São Carlos, SP, Brazil
²¹ Universidade de São Paulo, Instituto de Física, São Paulo, SP, Brazil
²² Universidade Estadual de Campinas (UNICAMP), IFGW, Campinas, SP, Brazil
²³ Universidade Estadual de Feira de Santana, Feira de Santana, Brazil
²⁴ Universidade Federal de Campina Grande, Centro de Ciencias e Tecnologia, Campina Grande, Brazil
²⁵ Universidade Federal do ABC, Santo André, SP, Brazil
²⁶ Universidade Federal do Paraná, Setor Palotina, Palotina, Brazil
²⁷ Universidade Federal do Rio de Janeiro, Instituto de Física, Rio de Janeiro, RJ, Brazil
²⁸ Universidad de Medellín, Medellín, Colombia
²⁹ Universidad Industrial de Santander, Bucaramanga, Colombia
³⁰ Charles University, Faculty of Mathematics and Physics, Institute of Particle and Nuclear Physics, Prague, Czech Republic
³¹ Institute of Physics of the Czech Academy of Sciences, Prague, Czech Republic
³² Palacky University, Olomouc, Czech Republic
³³ CNRS/IN2P3, IJCLab, Université Paris-Saclay, Orsay, France
³⁴ Laboratoire de Physique Nucléaire et de Hautes Energies (LPNHE), Sorbonne Université, Université de Paris, CNRS-IN2P3, Paris, France
³⁵ Univ. Grenoble Alpes, CNRS, Grenoble Institute of Engineering Univ. Grenoble Alpes, LPSC-IN2P3, 38000 Grenoble, France
³⁶ Université Paris-Saclay, CNRS/IN2P3, IJCLab, Orsay, France
³⁷ Bergische Universität Wuppertal, Department of Physics, Wuppertal, Germany
³⁸ Karlsruhe Institute of Technology (KIT), Institute for Experimental Particle Physics, Karlsruhe, Germany
³⁹ Karlsruhe Institute of Technology (KIT), Institut für Prozessdatenverarbeitung und Elektronik, Karlsruhe, Germany
⁴⁰ Karlsruhe Institute of Technology (KIT), Institute for Astroparticle Physics, Karlsruhe, Germany
⁴¹ RWTH Aachen University, III. Physikalischs Institut A, Aachen, Germany
⁴² Universität Hamburg, II. Institut für Theoretische Physik, Hamburg, Germany
⁴³ Universität Siegen, Department Physik – Experimentelle Teilchenphysik, Siegen, Germany
⁴⁴ Gran Sasso Science Institute, L'Aquila, Italy
⁴⁵ INFN Laboratori Nazionali del Gran Sasso, Assergi (L'Aquila), Italy
⁴⁶ INFN, Sezione di Catania, Catania, Italy
⁴⁷ INFN, Sezione di Lecce, Lecce, Italy
⁴⁸ INFN, Sezione di Milano, Milano, Italy
⁴⁹ INFN, Sezione di Napoli, Napoli, Italy
⁵⁰ INFN, Sezione di Roma "Tor Vergata", Roma, Italy
⁵¹ INFN, Sezione di Torino, Torino, Italy

- ⁵² Istituto di Astrofisica Spaziale e Fisica Cosmica di Palermo (INAF), Palermo, Italy
⁵³ Osservatorio Astrofisico di Torino (INAF), Torino, Italy
⁵⁴ Politecnico di Milano, Dipartimento di Scienze e Tecnologie Aerospaziali , Milano, Italy
⁵⁵ Università del Salento, Dipartimento di Matematica e Fisica “E. De Giorgi”, Lecce, Italy
⁵⁶ Università dell’Aquila, Dipartimento di Scienze Fisiche e Chimiche, L’Aquila, Italy
⁵⁷ Università di Catania, Dipartimento di Fisica e Astronomia “Ettore Majorana“, Catania, Italy
⁵⁸ Università di Milano, Dipartimento di Fisica, Milano, Italy
⁵⁹ Università di Napoli “Federico II”, Dipartimento di Fisica “Ettore Pancini”, Napoli, Italy
⁶⁰ Università di Palermo, Dipartimento di Fisica e Chimica ”E. Segrè”, Palermo, Italy
⁶¹ Università di Roma “Tor Vergata”, Dipartimento di Fisica, Roma, Italy
⁶² Università Torino, Dipartimento di Fisica, Torino, Italy
⁶³ Benemérita Universidad Autónoma de Puebla, Puebla, México
⁶⁴ Unidad Profesional Interdisciplinaria en Ingeniería y Tecnologías Avanzadas del Instituto Politécnico Nacional (UPIITA-IPN), México, D.F., México
⁶⁵ Universidad Autónoma de Chiapas, Tuxtla Gutiérrez, Chiapas, México
⁶⁶ Universidad Michoacana de San Nicolás de Hidalgo, Morelia, Michoacán, México
⁶⁷ Universidad Nacional Autónoma de México, México, D.F., México
⁶⁸ Institute of Nuclear Physics PAN, Krakow, Poland
⁶⁹ University of Łódź, Faculty of High-Energy Astrophysics, Łódź, Poland
⁷⁰ Laboratório de Instrumentação e Física Experimental de Partículas – LIP and Instituto Superior Técnico – IST, Universidade de Lisboa – UL, Lisboa, Portugal
⁷¹ “Horia Hulubei” National Institute for Physics and Nuclear Engineering, Bucharest-Magurele, Romania
⁷² Institute of Space Science, Bucharest-Magurele, Romania
⁷³ Center for Astrophysics and Cosmology (CAC), University of Nova Gorica, Nova Gorica, Slovenia
⁷⁴ Experimental Particle Physics Department, J. Stefan Institute, Ljubljana, Slovenia
⁷⁵ Universidad de Granada and C.A.F.P.E., Granada, Spain
⁷⁶ Instituto Galego de Física de Altas Enerxías (IGFAE), Universidade de Santiago de Compostela, Santiago de Compostela, Spain
⁷⁷ IMAPP, Radboud University Nijmegen, Nijmegen, The Netherlands
⁷⁸ Nationaal Instituut voor Kernfysica en Hoge Energie Fysica (NIKHEF), Science Park, Amsterdam, The Netherlands
⁷⁹ Stichting Astronomisch Onderzoek in Nederland (ASTRON), Dwingeloo, The Netherlands
⁸⁰ Universiteit van Amsterdam, Faculty of Science, Amsterdam, The Netherlands
⁸¹ Case Western Reserve University, Cleveland, OH, USA
⁸² Colorado School of Mines, Golden, CO, USA
⁸³ Department of Physics and Astronomy, Lehman College, City University of New York, Bronx, NY, USA
⁸⁴ Michigan Technological University, Houghton, MI, USA
⁸⁵ New York University, New York, NY, USA
⁸⁶ University of Chicago, Enrico Fermi Institute, Chicago, IL, USA
⁸⁷ University of Delaware, Department of Physics and Astronomy, Bartol Research Institute, Newark, DE, USA

^a Max-Planck-Institut für Radioastronomie, Bonn, Germany^b also at Kapteyn Institute, University of Groningen, Groningen, The Netherlands^c School of Physics and Astronomy, University of Leeds, Leeds, United Kingdom^d Fermi National Accelerator Laboratory, Fermilab, Batavia, IL, USA^e Pennsylvania State University, University Park, PA, USA^f Colorado State University, Fort Collins, CO, USA^g Louisiana State University, Baton Rouge, LA, USA^h now at Graduate School of Science, Osaka Metropolitan University, Osaka, Japanⁱ Institut universitaire de France (IUF), France^j now at Technische Universität Dortmund and Ruhr-Universität Bochum, Dortmund and Bochum, Germany

Acknowledgments

The successful installation, commissioning, and operation of the Pierre Auger Observatory would not have been possible without the strong commitment and effort from the technical and administrative staff in Malargüe. We are very grateful to the following agencies and organizations for financial support:

Argentina – Comisión Nacional de Energía Atómica; Agencia Nacional de Promoción Científica y Tecnológica (ANPCyT); Consejo Nacional de Investigaciones Científicas y Técnicas (CONICET); Gobierno de la Provincia de

Mendoza; Municipalidad de Malargüe; NDM Holdings and Valle Las Leñas; in gratitude for their continuing cooperation over land access; Australia – the Australian Research Council; Belgium – Fonds de la Recherche Scientifique (FNRS); Research Foundation Flanders (FWO), Marie Curie Action of the European Union Grant No. 101107047; Brazil – Conselho Nacional de Desenvolvimento Científico e Tecnológico (CNPq); Financiadora de Estudos e Projetos (FINEP); Fundação de Amparo à Pesquisa do Estado de Rio de Janeiro (FAPERJ); São Paulo Research Foundation (FAPESP) Grants No. 2019/10151-2, No. 2010/07359-6 and No. 1999/05404-3; Ministério da Ciência, Tecnologia, Inovações e Comunicações (MCTIC); Czech Republic – GACR 24-13049S, CAS LQ100102401, MEYS LM2023032, CZ.02.1.01/0.0/0.0/16_013/0001402, CZ.02.1.01/0.0/0.0/18_046/0016010 and CZ.02.1.01/0.0/0.0/17_049/0008422 and CZ.02.01.01/00/22_008/0004632; France – Centre de Calcul IN2P3/CNRS; Centre National de la Recherche Scientifique (CNRS); Conseil Régional Ile-de-France; Département Physique Nucléaire et Corpusculaire (PNC-IN2P3/CNRS); Département Sciences de l'Univers (SDU-INSU/CNRS); Institut Lagrange de Paris (ILP) Grant No. LABEX ANR-10-LABX-63 within the Investissements d'Avenir Programme Grant No. ANR-11-IDEX-0004-02; Germany – Bundesministerium für Bildung und Forschung (BMBF); Deutsche Forschungsgemeinschaft (DFG); Finanzministerium Baden-Württemberg; Helmholtz Alliance for Astroparticle Physics (HAP); Helmholtz-Gemeinschaft Deutscher Forschungszentren (HGF); Ministerium für Kultur und Wissenschaft des Landes Nordrhein-Westfalen; Ministerium für Wissenschaft, Forschung und Kunst des Landes Baden-Württemberg; Italy – Istituto Nazionale di Fisica Nucleare (INFN); Istituto Nazionale di Astrofisica (INAF); Ministero dell'Università e della Ricerca (MUR); CETEMPS Center of Excellence; Ministero degli Affari Esteri (MAE), ICSC Centro Nazionale di Ricerca in High Performance Computing, Big Data and Quantum Computing, funded by European Union NextGenerationEU, reference code CN_00000013; México – Consejo Nacional de Ciencia y Tecnología (CONACYT) No. 167733; Universidad Nacional Autónoma de México (UNAM); PAPIIT DGAPA-UNAM; The Netherlands – Ministry of Education, Culture and Science; Netherlands Organisation for Scientific Research (NWO); Dutch national e-infrastructure with the support of SURF Cooperative; Poland – Ministry of Education and Science, grants No. DIR/WK/2018/11 and 2022/WK/12; National Science Centre, grants No. 2016/22/M/ST9/00198, 2016/23/B/ST9/01635, 2020/39/B/ST9/01398, and 2022/45/B/ST9/02163; Portugal – Portuguese national funds and FEDER funds within Programa Operacional Factores de Competitividade through Fundação para a Ciéncia e a Tecnologia (COMPETE); Romania – Ministry of Research, Innovation and Digitization, CNCS-UEFISCDI, contract no. 30N/2023 under Romanian National Core Program LAPLAS VII, grant no. PN 23 21 01 02 and project number PN-III-P1-1.1-TE-2021-0924/TE57/2022, within PNCDI III; Slovenia – Slovenian Research Agency, grants P1-0031, P1-0385, I0-0033, NI-0111; Spain – Ministerio de Ciencia e Innovación/Agenzia Estatal de Investigación (PID2019-105544GB-I00, PID2022-140510NB-I00 and RYC2019-027017-I), Xunta de Galicia (CIGUS Network of Research Centers, Consolidación 2021 GRC GI-2033, ED431C-2021/22 and ED431F-2022/15), Junta de Andalucía (SOMM17/6104/UGR and P18-FR-4314), and the European Union (Marie Skłodowska-Curie 101065027 and ERDF); USA – Department of Energy, Contracts No. DE-AC02-07CH11359, No. DE-FR02-04ER41300, No. DE-FG02-99ER41107 and No. DE-SC0011689; National Science Foundation, Grant No. 0450696, and NSF-2013199; The Grainger Foundation; Marie Curie-IRSES/EPLANET; European Particle Physics Latin American Network; and UNESCO.